Inorg. Chem. **2005**, *44*, 1006–1014

Thermodynamic Profiles for CO Photodissociation from Heme Model Compounds: Effect of Proximal Ligands†

Jaroslava Mikšovská, Jeni Norstrom, and Randy W. Larsen*

Department of Chemistry, University of South Florida, 4202 E. Fowler Av. SCA 400, Tampa, Florida 33620

Received July 30, 2004

Here we present a comprehensive study of the thermodynamic parameters (enthalpy, entropy, and volume changes) associated with carbon monoxide photodissociation and rebinding to Fe(II) microperoxidase-11 (Fe^{II}MP11) and Fe(II) tetrakis(4-sulfonatophenyl)porphine complex (Fe^{II}4SP) with water and 2-methylimidazole as proximal ligands. CO photodissociation from Fe^{II}4SP complexes is accompanied by a positive volume change of $\sim$ 17 mL mol^{-1}. A smaller volume change of $\sim$12 mL mol^{-1} was observed for CO dissociation from Fe^{II}MP-11. We attribute the positive volume change to cleavage of the Fe–CO covalent bond and to solvent reorganization due to the low-spin to high-spin transition. CO binding is an exothermic reaction with an enthalpy change of –17 kcal mol^{-1} for the CO–Fe^{II}4SP complexes and –13 kcal mol^{-1} for the CO–Fe^{II}MP11 complex. In all cases, the ligand recombination occurs as a single-exponential process indicating that CO dissociation is followed by direct CO rebinding to a high-spin five-coordinate complex without concomitant dissociation of the proximal base. In addition, observed negative activation entropies and volumes for ligand binding to (2-MeIm)Fe^{II}4SP and MP-11, respectively, suggest that CO rebinding can be described by an associative mechanism with bond formation being the rate-limiting step.

Introduction

Metalloporphyrins form a diverse class of molecules capable of catalyzing a wide range of chemical processes including oxidations, peroxide degradation, hydroxylations, and electron transport.[1−3] These macrocycles are also key components in light-harvesting dyads and in photodynamic therapy agents. Nature takes full advantage of the catalytic versatility of metalloporphyrins by incorporating iron porphyrins in a plethora of protein complexes. These complexes perform critical biological functions such as oxygen transport and storage (hemoglobins/myoglobins), oxygen reduction (terminal heme/copper oxidases), electron transfer (*b*- and *c*-type cytochromes, etc.), monooxygenation (Cyt P_{450}), and peroxide/superoxide scavenging (catalases and peroxidases). Nearly all of these proteins contain the same iron porphyrin macrocycle Fe(2+/3+) protoporphyrin IX. The catalytic versatility in these proteins arises from a complex balance of proximal ligation and distal heme pocket environment.

Binding of diatomic ligands to heme cofactors has been intensively studied to elucidate the mechanism of ligand binding and activation in heme proteins. A large number of spectroscopic studies have been performed to probe the heme dynamics associated with CO and O_2 binding to various iron porphyrins solubilized in organic solvents or in detergent micelles.[1,5−9] To mimic the ligand binding to heme proteins such as myoglobin and hemoglobin, these model heme compounds contained nitrogen-based ligands including imidazole, 1-methylmidazole, and 2-methylimidazole. Kinetics of CO association to various heme compounds have been studied

* Author to whom correspondence should be addressed. E-mail: rlarsen@cas.usf.edu.

† Abbreviations: L, ligand; 2-MeIm, 2-methylimidazole; Fe^{III}4SP, Fe(III) tetrakis(4-sulfonatophenyl)porphine; MP-11, microperoxidase 11; PAC, photoacoustic calorimetry; PBD, photothermal beam deflection; TA, transient absorption.

(1) Traylor, T. G. *Pure Appl. Chem.* **1991**, *63*, 265.
(2) Reedy, C. J.; Gibney, B. R. *Chem. Rev.* **2004**, *104*, 617−650.
(3) Sono, M.; Roach, M. P.; Coulter, E. D.; Dawson, J. H. **1996**, *96*, 2841−2888.
(4) Gouterma, M. In *The Porphyrins*; Dolphin, D., Ed.; Academic Press: New York, 1978; Part I.
(5) Spiro, T. G. In *Iron Porphyrins*; Lever, A. B. P., Gray, H. B., Eds.; Addison-Wesley: Reading, MA, 1983.
(6) White, D. K.; Cannon, J. B.; Traylor, T. G. *J. Am. Chem. Soc.* **1979**, *101*, 2443−2454.
(7) Traylor, T. G. *Acc. Chem. Res.* **1981**, *14*, 102−109.
(8) Traylor, T. G.; Luo, J.; Simon, J. A.; Ford, P. C. *J. Am. Chem. Soc.* **1992**, *114*, 4340−4345.
(9) Huang, Y.; Marden, M. C.; Lambry, J. C.; Fontain-Aupart, M. P.; Pansu, R.; Martin, J. L.; Poyart, C. *J. Am. Chem. Soc.* **1991**, *113*, 9141−9144.

10.1021/ic048963c CCC: $30.25
Published on Web 01/15/2005

by nanosecond laser photolysis, and the "base elimination" pathway for CO rebinding has been proposed.[6,9] On the other hand, chelated protohemes and other unstrained chelated hemes are believed to react predominantly by the direct association mechanism in organic solvents or in aqueous medium.[7]

In our group we use photothermal methods together with transient absorption spectroscopy to obtain complete thermodynamic profiles for ligand binding to heme proteins and heme model compounds. Previously we have characterized volume and enthalpy changes coupled to CO binding to a heme model system composed of protoporphyrin IX (Fe^{II}PPIX) encapsulated in cetylmethylammonium bromide (CTAB) micelles.[10] Using PAC together with time-resolved absorption spectroscopy (TA) we have shown that CO photodissociation from the $(CO)(H_2O)Fe^{II}$PPIX/CTAB complex results in formation of a four-coordinated complex that is accompanied by a volume decrease of -3 mL mol^{-1} and an enthalpy change of -10 kcal mol^{-1}. Subsequent ligand recombination occurs as a simultaneous rebinding of both CO and H_2O ligands.

Recently we have determined reaction and activation volume and enthalpy changes associated with the CO binding to a water-soluble Fe(II) *meso*-tetrakis(4-sulfonatophenyl)-porphyrin (Fe^{II}4SP) using PBD and transient absorption spectroscopy.[11] In this study we report the complete thermodynamic profiles for CO photodissociation and subsequent rebinding to Fe^{II}4SP in the presence of water or 2-methylimidazole as proximal ligands. Hindered bases such as 2-methylimidazole have been previously used to model reactions of the strained hemoglobin T state because the binding of hindered base to heme results in porphyrin ring doming.[6,12] In addition, we have determined a thermodynamic profile for CO photodissociation and rebinding to microperoxidase 11 (MP11). Microperoxidase 11 is an 11 residue heme-binding peptide obtained by proteolytic digestion of horse heart cytochrome *c*.[13] Heme is covalently bond to the peptide via thioether linkages involving two cysteine residues and coordinated through His18 making MP-11 a good five-coordinate heme protein model.

Using PAC and PBD we have characterized reaction volume and enthalpy changes associated with the CO photodissociation and subsequent rebinding to $(H_2O)Fe^{II}$4SP, (2-MeIm)Fe^{II}4SP, and Fe^{II}MP-11 complexes. Our results show that the low-spin to high-spin heme transition is accompanied by an expansion of $\sim$17 mL mol^{-1} for Fe^{II}4SP complexes and smaller volume change of $\sim$12 mL mol^{-1} for MP-11. We discuss the origin of observed volume changes in terms of volume change due to the different solvation of the high-spin and low-spin heme. Only one kinetic phase was observed in transient absorption and PBD measurements on the time scale longer than 50 ns indicating that CO rebinds directly to five-coordinate heme and the reaction involves only Fe$-$CO bond formation. That is confirmed by observed negative activation volumes and entropies for ligand rebinding underlying the associative mechanism of the reaction.

Materials and Methods

Fe^{III}4SP was purchased from Porphyrin Products Inc., microperoxidase 11 (MP-11) and 2-methylimidazole were obtained from Sigma-Aldrich, and sodium dithionite was from Fisher. Samples were prepared by diluting Fe^{III}4SP or MP-11 in 50 mM Tris buffer (pH = 7.5) from stock solutions to obtain a final concentration of $\sim$10 μM for photothermal measurements and $\sim$4 μM for TA measurements. The concentration of Fe^{III}4SP was calculated using $\epsilon_{392} = 155$ mM^{-1} cm^{-1}.[14] The complex with 2-methylimidazole was prepared by dissolving Fe^{III}4SP in 50 mM Tris buffer containing 50 mM 2-MeIm. The cuvette was then sealed with a septum cap and purged with Ar for $\sim$30 min. A small amount of sodium dithionite was added to reduce the sample. Finally, the sample was purged with CO for approximately 5 min. CO association constants were determined by spectrometric titration. Titrations were performed by sequentially adding saturated aqueous CO to a solution of ferrous heme complex and recording absorbance changes in the spectral region between 300 and 700 nm using a double beam UV-2401 Shimadzu spectrophotometer.

Volume and enthalpy changes following ligand dissociation were measured using photoacoustic calorimetry (PAC) and photothermal beam deflection (PBD). The PAC and PBD setups have been described in detail elsewhere.[15,16] Typically, 30$-$50 laser pulses were averaged per trace over a temperature range from 16 to 35 °C. Excitation was provided by a frequency doubled Nd:YAG laser (532 nm, 7 ns pulse, $<$100 μJ/pulse, 1 Hz repetition rate) (Minilite I, Continuum). We used Fe^{III}4SP in 50 mM Tris buffer pH 7.5 as a calorimetric reference compound for photothermal measurements. Its absorbance matched the absorbance of the sample at the excitation wavelength ($A_{532nm} \sim 0.4$).

Transient absorption studies were carried out on a homemade instrument. The probe beam from the arc of a 150 W Xe arc lamp (Thermo-Oriel) is passed through a MC1-02 single monochromator (Optometrics USA) and centered on the sample placed in either a temperature controlled cuvette holder (Quantum Northwest) or in a high-pressure cell (ISS, Urbana-Champagne, IL). Light emerging from the sample is then focused on the slit of a second monochromator (H10, Jobin Yvon) and detected by a PMT (H6780, Hamamatsu) coupled to a high gain amplifier (70710, Thermo-Oriel). The signal is then digitized using a 4 GHz transient digitizer (TDS 7404, Tektronix). The photochemistry was initiated by a 532 nm pulse from a frequency doubled Nd:YAG laser (Leopard D-20, Continuum) with 20 ps pulse width and 20 Hz repetition.

Analysis of PAC and PBD Signals. The amplitude of the photoacoustic signal, *S*, was determined as a difference between the first maximum and minimum in the signal and can be expressed as[15,16]

$$S = KE_a\Phi(\Delta V_{thermal} + \Delta V_{nonthermal}) \quad (1)$$

where *K* is an instrument response parameter, E_a is the number of

(10) Larsen, R. W. *Inorg. Chim. Acta* **1998**, *288*, 74$-$81.
(11) Barker, B. D.; Larsen, R. W. *J. Inorg. Biochem.* **2001**, *85*, 107$-$116.
(12) Collman, J. P.; Brauman, J. I.; Doxsee, K. M.; Halbert, T. R.; Suslick, K. S. *J. Am. Chem. Soc.* **1978**, *100*, 2761$-$2766.
(13) Urry, D. W. *J. Biol. Chem.* **1967**, *242*, 4441$-$4448.
(14) Owens, J. W.; Robinson, J.; O'Connor, C. J. *Inorg. Chim. Acta* **1993**, *206*, 141$-$153.
(15) Barker, B. D.; Larsen, R. W. *J. Biochem. Mol. Biol. Biophys.* **2001**, *5*, 407$-$434.
(16) Mikšovská, J.; Larsen, R. W. In *Methods in Enzymology: Vol. 360 Biophotonics*; Marriott, G., Parker, I., Eds.; Academic Press: New York, 2003; Part A.

Einsteins absorbed, Φ is the quantum yield, $\Delta V_{\text{thermal}}$ represents the volume change due to the radiationless relaxation, and $\Delta V_{\text{nonthermal}}$ describes the volume change due to the induced photochemical processes. $\Delta V_{\text{thermal}}$ is proportional to the heat released into solution according to

$$\Delta V_{\text{thermal}} = Q(\beta/C_p\rho) \tag{2}$$

where Q is the heat released to the solvent, β is the coefficient of thermal expansion of the solvent (K^{-1}), C_p is the heat capacity (cal $g^{-1}K^{-1}$), and ρ is the density (g mL^{-1}). The instrument response parameter can be eliminated by employing a calorimetric reference compound that promptly converts the energy of the absorbed photon, $E_{h\nu}$, into heat with a quantum yield of unity and which undergoes no structural changes. The amplitude of the acoustic signal for the reference compound is then described as

$$R = KE_aE_{h\nu}(\beta/C_p\rho) \tag{3}$$

and the ratio of the sample signal to the reference signal gives the following expression:

$$(S/R)E_{h\nu} = \Phi[Q + (\Delta V_{\text{nonthermal}}/(\beta/C_p\rho)] \tag{4}$$

A plot of $(S/R)E_{h\nu}$ versus $C_p\rho/\beta$ gives a straight line with a slope equal to $\Phi V_{\text{nonthermal}}$ and an intercept equal to the released heat (Q). Subtracting ΦQ from $E_{h\nu}$ gives ΔH for the reaction.

The corresponding PBD signal can be described as[17]

$$S = KE_a\Phi[(dn/dt)(1/\rho C_p)Q + \rho(dn/d\rho)\Delta V) + B\Delta n_{\text{abs}}] \tag{5}$$

where n is the refractive index of the solution and $B\Delta n_{\text{abs}}$ is the change in the refractive index due to the absorption changes in the sample. To eliminate the instrument response parameter the signal of an appropriate reference compound is measured at identical temperatures, and the reference magnitude is

$$R = KE_aE_{h\nu}[(dn/dt)(1/\rho C_p)]Q \tag{6}$$

The ratio of the sample signal to the reference signal gives the following expression:

$$(S/R)E_{h\nu} = \Phi Q + \Phi[\rho(dn/d\rho)\Delta V_{\text{con}} + B\Delta n_{\text{abs}}]/(dn/dt)(1/\rho C_p) \tag{7}$$

As long as the probe laser wavelength is far from any absorption band of the molecule (including any transient absorption bands that may appear during a photochemical process), $B\Delta n_{\text{abs}}$ will be small and can be neglected. The term $\rho(dn/d\rho)$ is constant in the temperature range between 0 and 35 °C ($\rho(dn/d\rho) = 0.326 \pm 0.001$).[17] Then, from a plot of S/R scaled to $E_{h\nu}$, the released heat (ΦQ) and volume change ($\Phi\Delta V$) can be obtained.

Volume and enthalpy parameters of individual reaction steps can be obtained by fitting PBD traces to the following equation:

$$F = \alpha_0 + \Sigma\alpha_i(1 - \exp(t/\tau_i) \tag{8}$$

Here α_i is equivalent to S in eq 5 for each intermediate step and τ_i are the corresponding lifetimes.

From a temperature dependence of the observed rate constants ($k_i = 1/\tau_i$) the activation enthalpy and entropy changes can be calculated by using the following equation:

$$\ln(k_{\text{obs}}T/k_bh) = \Delta S^{\ddagger}/R - \Delta H^{\ddagger}/RT \tag{9}$$

Here k_b is Boltzmann's constant, h is Planck's constant, k_{obs} is the observed rate constant, and T is the absolute temperature. The corresponding volumes of activation were determined by plotting ln k_{obs} versus pressure using[18,19]

$$\Delta V^{\ddagger} = -(\delta(\ln k)/\delta P)RT \tag{10}$$

where P is pressure and R is the gas constant.

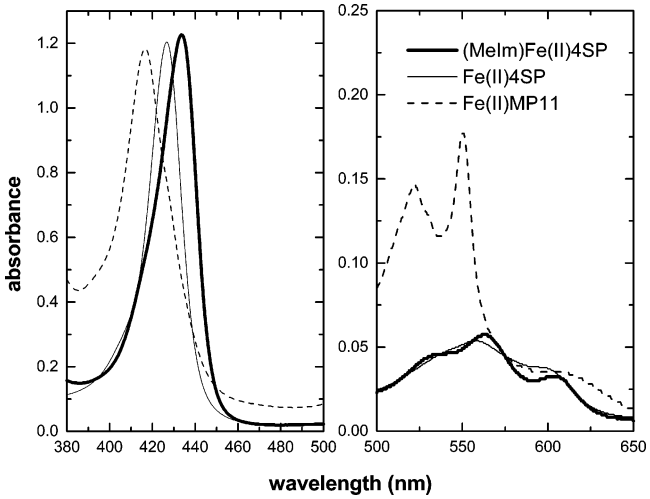

Figure 1. Steady-state UV−vis spectra of Fe^{II}4SP, (2-MeIm)Fe^{II}4SP, and Fe^{II}MP-11. Samples were prepared by reducing Fe^{III}4SP or -MP-11 in 50 mM Tris buffer (pH 7.5) and in the presence of 50 mM 2-methylimidazole for the (2-MeIm)Fe^{II}4SP complex. The spectra are normalized to the absorbance value of the Soret band.

Results

Steady-State UV−Vis Spectroscopy. Steady-state absorption spectra of reduced Fe^{II}4SP in water and in the presence of 50 mM 2-MeIm are shown in Figure 1 together with the spectrum of reduced MP-11. Fe^{II}4SP in water, pH 7.5, exhibits a Soret band at 426 nm and a single band at 558 nm with a long-wavelength shoulder that corresponds to the formation of a high-spin five-coordinate complex (H_2O)Fe^{II}4SP.[11] In the presence of 50 mM 2-MeIm a high-spin five-coordinate (2-MeIm)Fe^{II}4SP is formed[20] and is characterized by the presence of a Soret band at 433 nm and a shift of the band in the visible region of the spectrum to 564 nm. Reduced MP-11 exhibits an UV−vis spectrum with a Soret band maximum at 416 nm and two peaks at 520 and 550 nm, which is characteristic of a low-spin six-coordinated complex. It has been postulated that the sixth ligand may be provided by the terminal amino group of the same molecule and/or aggregation of different MP-11 molecules.[21] Figure 2 shows that CO addition leads to the formation of six-coordinate (CO)(L)Fe^{II} complexes with Soret bands situated at 412, 415, and 417 nm for the (CO)Fe^{II}MP-11, (CO)(H_2O)Fe^{II}4SP, and (CO)(2-MeIm)-Fe^{II}4SP complexes, respectively.

(17) Schulenber, P. J.; Gartner, W.; Braslavsky, S. E. *J. Phys. Chem.* **1995**, *99*, 9617−9624.
(18) Van Eldik, R.; Asano, T.; le Noble, W. *Chem. Rev.* **1989**, *89*, 549−688.
(19) Drljaca, A.; Hubbard, C. D.; van Eldik, R.; Asano, T.; Basilevsky, M. V.; le Noble, W. J. *Chem. Rev.* **1998**, *9*, 2167−2290.
(20) Wagner, G. C.; Kassner, R. J. *Biochim. Biophys. Acta* **1975**, *392*, 319−327.
(21) Jehanly, A. M.; Stotter, D. A.; Wilson, M. T. *Eur. J. Biochem.* **1976**, *71*, 613−616.

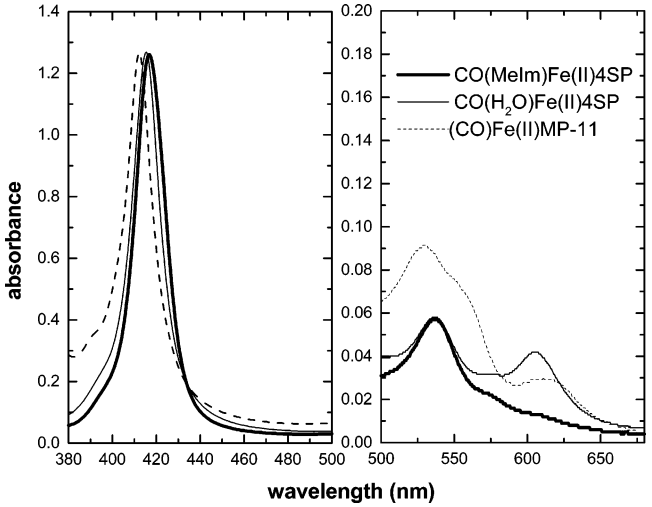

Figure 2. Steady-state absorption spectra of the $(CO)(H_2O)Fe^{II}4SP$, $(CO)(2\text{-MeIm})Fe^{II}4SP$, and $(CO)Fe^{II}MP\text{-}11$ complexes. Samples were prepared by purging reduced complexes in Figure 1 with CO.

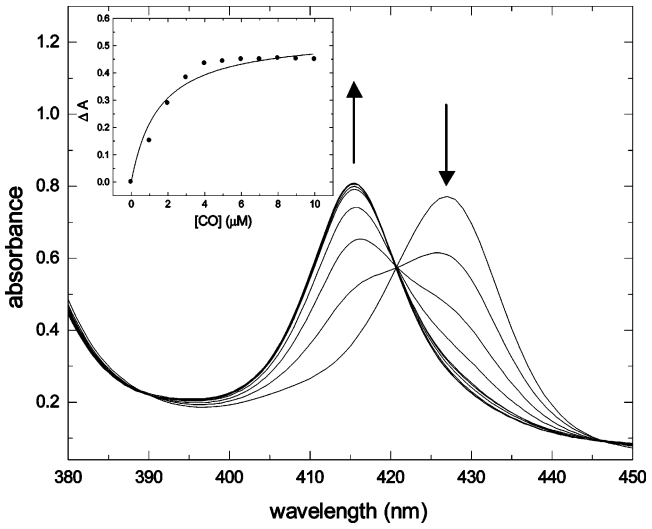

Figure 3. UV−Vis spectra of ~3 μM $Fe^{II}4SP$ in 50 mM Tris buffer pH 7.5 as a function of CO concentration (1−10 μM). The inset shows the plot of ΔA versus [CO] at 414 nm. The solid line corresponds to the best fit according to eq 11 in the text.

CO association constants were determined from absorption changes upon ligand additions. Figure 3 displays absorption spectra of $(H_2O)Fe^{II}4SP$ as a function of CO concentration (data for $(2\text{-MeIm})Fe^{II}4SP$ and $Fe^{II}MP11$ not shown). CO additions result in a hypsochromic shift of the Soret band and a well-defined isosbestic point consistent with the presence of two absorbing species in solution. Association constants (K_a) were found by assuming a simple two-step equilibrium in all cases: $CO + (L)Fe^{II}P \leftrightarrow (CO)(L)Fe^{II}P$. Using the change in absorbance as a function of CO concentration allows for the determination of K_a from

$$\Delta A = K_a * \Delta\epsilon * c * [CO]/(1 + K_a[CO]) \qquad (11)$$

where $\Delta\epsilon$ is the change in molar extinction coefficient at the monitoring wavelength, c is the initial concentration of iron porphyrin, and [CO] is the solution concentration of CO. Fits of the titration data to eq 11 give K_a values between 5×10^5 and 2×10^6 M^{-1} and are summarized in Table 1.

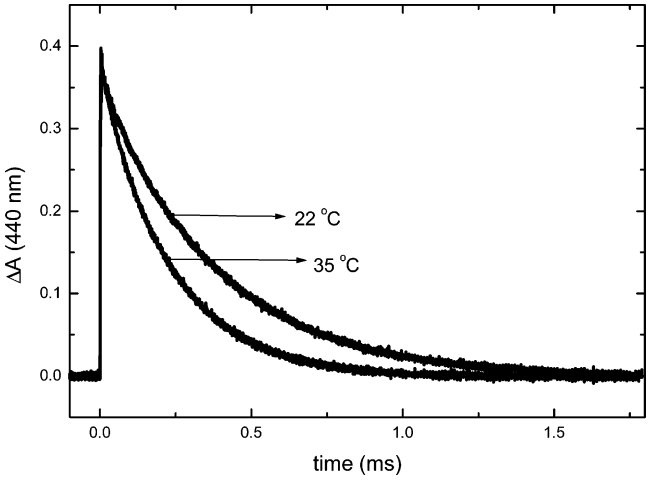

Figure 4. Transient absorption traces for CO rebinding to $(2\text{-MeIm})Fe^{II}4SP$ at 22 and 35 °C.

Table 1. Association Constants, $\Delta G°$, and $\Delta S°$ for CO Binding to $(H_2O)Fe^{II}4SP$, $(2\text{-MeIm})Fe^{II}4SP$, and $Fe^{II}MP11$

	K_{CO} (M^{-1})	$\Delta G°$ (kcal mol^{-1})	$\Delta S°$ (cal K^{-1} mol^{-1})
$(H_2O)Fe^{II}4SP$	$(5.1 \pm 1.0) \times 10^5$	-7.8 ± 0.1	-28
$(2\text{-MeIm})Fe^{II}4SP$	$(5.3 \pm 0.5) \times 10^5$	-7.8 ± 0.1	-28
$Fe^{II}MP\text{-}11$	$(1.9 \pm 0.2) \times 10^6$	-8.4 ± 0.1	-19

The association constants were used to determine corresponding $\Delta G°$ values. From these values and using reaction enthalpy values obtained from PAC and PBD measurements (see below), reaction entropy changes for CO association were calculated and are listed in Table 1.

Temperature-/Pressure-Dependent Transient Absorption. In a previous study from our group we reported that after ligand photodisociation from the $(CO)(H_2O)Fe^{II}4SP$ complex CO rebinds in a single-exponential step with a pseudo-first-order rate constant of 2.5×10^4 s^{-1} (20 °C, 1 mM CO). Transient absorption traces for CO rebinding to $(2\text{-MeIm})Fe^{II}4SP$ also reveal single-exponential decay kinetics with a rate constant of 2.5×10^3 s^{-1} (1 mM CO) which is about 1 order of magnitude smaller than the rate constant for CO rebinding to $(H_2O)Fe^{II}4SP$ (Figure 4). As in the case of the $Fe^{II}4SP$ complexes, transient absorption traces for CO recombination to $Fe^{II}MP\text{-}11$ follows single-exponential decay kinetics characterized by a rate constant of 9.7×10^3 s^{-1} at 20 °C. The absence of any additional kinetics in this case indicates that CO rebinding must occur faster than the rebinding of either an intra- or intermolecular ligand which is present in the reduced MP-11 under steady-state conditions. From temperature-dependent measurements the activation enthalpy and entropy changes were determined (Eyring plot in Figure 5). Extrapolated values are summarized in Table 2. From the corresponding pressure dependent measurements of the rate constants for CO rebinding, the volumes of activation were extrapolated according to eq 10. Figure 6 shows a plot of ln k_{obs} versus pressure for ligand recombination to $(2\text{-MeIm})Fe^{II}4SP$ and MP-11, and extrapolated values for the activation volume changes are listed in Table 2.

PAC and PBD Measurements. Reaction volume and enthalpy changes have been determined using PAC for the CO photodissociation reaction and by PBD for both the

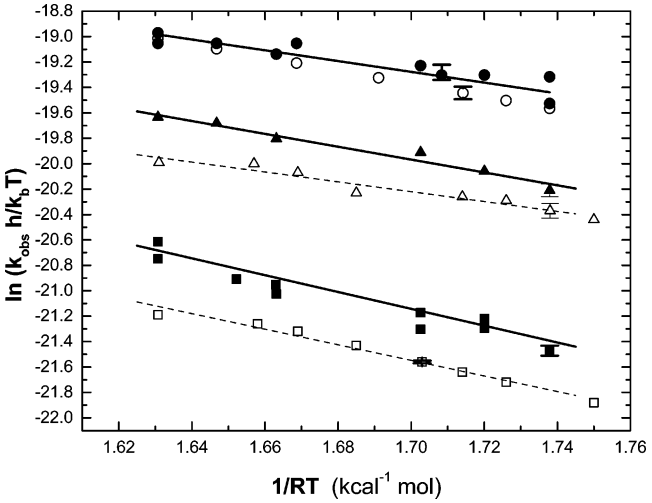

Figure 5. Eyring plot for the CO rebinding after photolysis of (CO)(H_2O)Fe^{II}4SP (circles), (CO)(2-MeIm)Fe^{II}4SP (squares), and (CO)-Fe^{II}MP-11 (triangles). The data from TA measurement are shown as open symbols, and the data from PBD measurements, as closed symbols. Extrapolated values of $\Delta H^{\ddagger}$ and $\Delta S^{\ddagger}$ are listed in Table 2.

Table 2. Activation Parameters for CO Rebinding Reaction Obtained from PBD and TA Measurements[a]

	$\Delta H^{\ddagger}$ (kcal mol^{-1})		$\Delta S^{\ddagger}$ (cal K^{-1} mol^{-1})		$\Delta V^{\ddagger}$ (mL mol^{-1})
	TA	PBD	TA	PBD	for TA
$H_2O$$Fe^{II}$4SP	3.9 ± 0.3	3.7 ± 0.5	-11 ± 2	-12.9 ± 0.8	nd
2-MeImFe^{II}4SP	6.6 ± 0.2	6.7 ± 0.6	-10.3 ± 0.2	-10 ± 1.0	-11 ± 2
Fe^{II}MP-11	3.9 ± 0.4	5.0 ± 0.7	-13.6 ± 0.7	-11.3 ± 0.9	-17 ± 3

[a] See text for details.

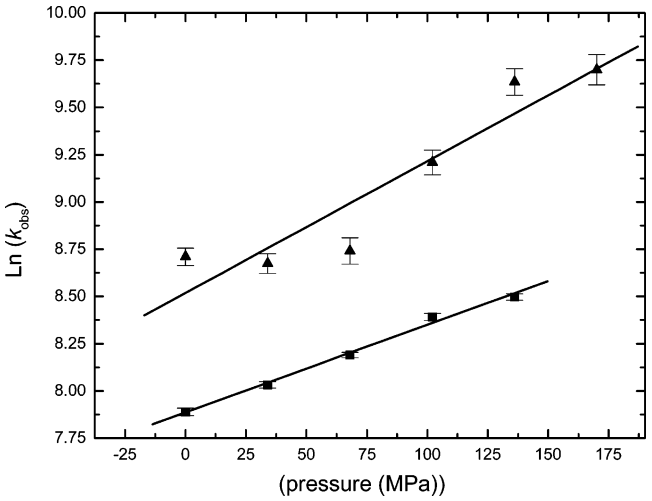

Figure 6. Pressure dependence for CO recombination to (CO)(2-MeIm)-Fe^{II}4SP (squares) and (CO)Fe^{II}MP-11 (triangles).

Table 3. Reaction Volume and Enthalpy Changes for CO Photodissociation from (CO)(L)Fe^{II}4SP Obtained from PAC Measurements

	ΔV (mL mol^{-1})	ΔH (kcal mol^{-1})
(H_2O)Fe^{II}4SP	18 ± 1.0	20 ± 4
(2-MeIm)Fe^{II}4SP	21.1 ± 0.7	17 ± 3
Fe^{II}MP-11	11.2 ± 0.9	13.0 ± 3

dissociation and rebinding reactions (Tables 3 and 4). Overlays of acoustic waves for CO photodissociation from (CO)-(H_2O)Fe^{II}4SP, (CO)(2-MeIm)Fe^{II}4SP, and (CO)Fe^{II}MP11 and the corresponding reference traces at 22 °C are shown in

Table 4. Reaction Volume and Enthalpy Changes for CO Photodissociation and Subsequent Rebinding Obtained from PBD Measurements

	$\Delta V_{fastphase}$ (mL mol^{-1})	$\Delta H_{fastphase}$ (kcal mol^{-1})	$\Delta V_{slowphase}$ (mL mol^{-1})	$\Delta H_{slowphase}$ (kcal mol^{-1})
(H_2O)Fe^{II}4SP	16 ± 1	9 ± 4	-17 ± 2	-20 ± 3
(2-MeIm)Fe^{II}4SP	17 ± 2	16 ± 7	-18 ± 3	-16 ± 9
Fe^{II}MP-11	12 ± 3	17 ± 6	-11 ± 2	-11 ± 6

Figure 7. The absence of any phase shift in the acoustic wave of the sample relative to the reference acoustic wave indicates that volume and enthalpy changes associated with CO photolysis occur on a time scale faster than the response time of the acoustic detector (<50 ns) and that there are no additional volume/enthalpy changes between 50 ns and ~5 μs. Plots of the ratio of the amplitude of the sample acoustic

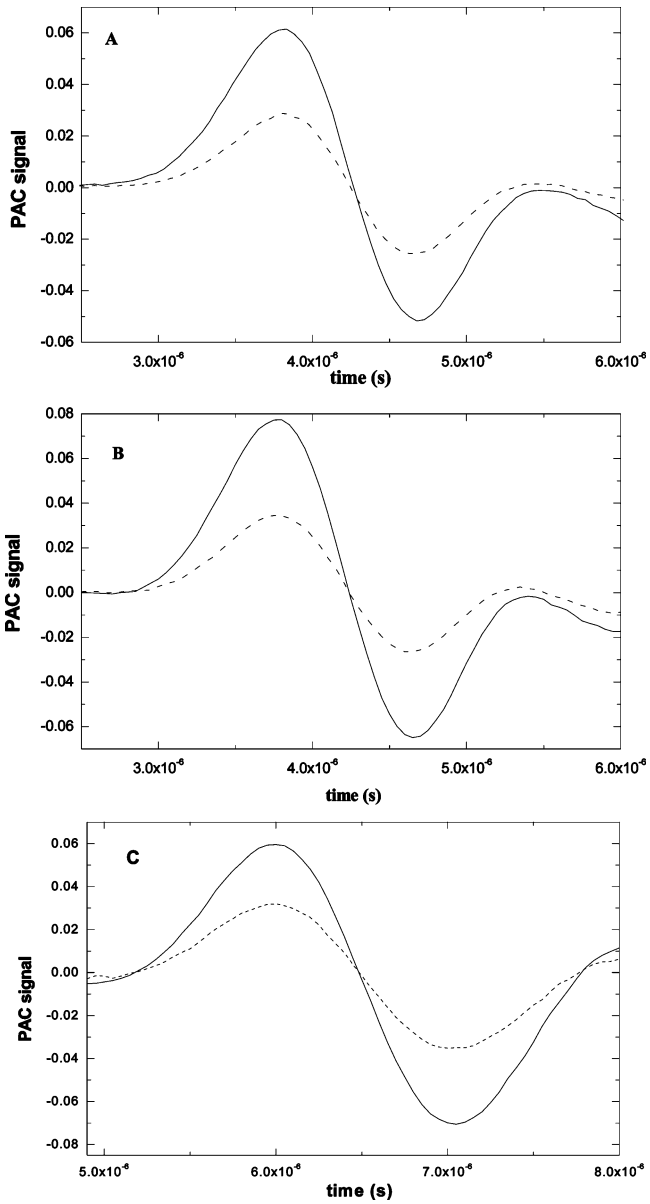

Figure 7. PAC traces for CO photodissociation from (A) (CO)-(H_2O)Fe^{II}4SP, (B) (CO)(2-MeIm)Fe^{II}4SP, and (C) (CO)Fe^{II}MP-11 complexes at 22 °C. The sample traces are shown as solid lines, and the reference traces, as dashed lines. The absorbance of the sample and the reference (Fe^{III}4SP in 50 mM Tris buffer, pH 7) at 532 nm was ~0.35. Samples were prepared as described in Materials and Methods.

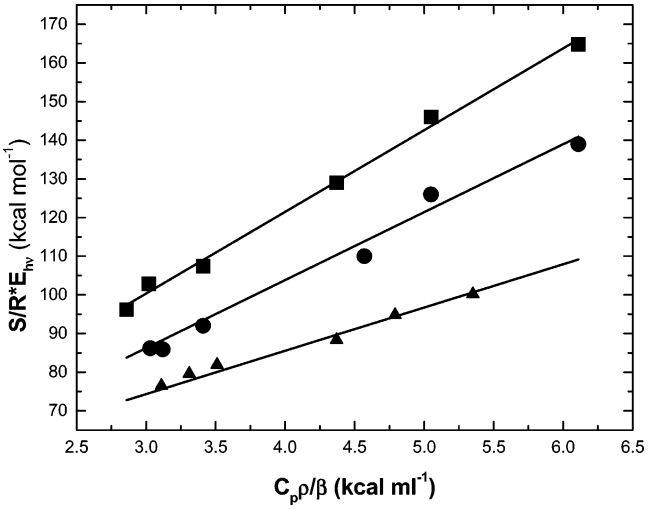

Figure 8. Plot of $S/R^*E_{h\nu}$ versus $C_p\rho/\beta$ for CO photodissociation from the (CO)(H_2O)Fe^{II}4SP (circles), (CO)(2-MeIm)Fe^{II}4SP (squares), and (CO)Fe^{II}MP-11 (triangles) complexes.

wave to the amplitude of the reference acoustic wave versus ($C_p\rho/\beta$) give a straight line as shown in Figure 8. According to eq 3, the reaction volume change and heat release to the solvent (Q) can be obtained from the slope and intercept of the line, respectively. The enthalpy change is calculated from Q using

$$\Delta H = E_{h\nu} - Q \tag{12}$$

where $E_{h\nu} = 53.73$ kcal mol^{-1}. The volume and enthalpy changes accompanying ligand dissociation from the (CO)(L)Fe^{II}4SP complexes are summarized in Table 1.

PBD allows volume and enthalpy changes to be observed on the microsecond to millisecond time scale; thus, the volume and enthalpy changes for CO rebinding can be determined from the amplitude of the slow phase. In addition, the integrated volume and enthalpy changes occurring faster than the resolution of the PBD instrument ($\sim$10 μs) can be determined from the amplitude of the fast phase. Figure 9 shows PBD traces after CO photodissociation from (CO)-(H_2O)Fe^{II}4SP, (CO)(2-MeIm)Fe^{II}4SP, and (CO)Fe^{II}MP11 complexes as well as the corresponding ligand rebinding. From the temperature dependence of the fast and slow phase PBD amplitudes normalized to the amplitude of the reference compound the volume changes were determined (eq 7). Enthalpy changes for the fast phase were determined according to eq 11, and enthalpy changes for the slow phase were obtained from $\Delta H = -Q$. Plots of α_i/R versus $C_p\rho/(dn/dt)$ for all complexes examined are shown in Figure 10, and extrapolated values are listed in Table 2. The volume and enthalpy changes obtained from the fast phase of the PBD traces should match those determined by the PAC measurements. In addition, since CO dissociation and rebinding is a reversible reaction, the values determined for the CO rebinding should be of the same magnitude but opposite sign of values obtained for CO dissociation. The volume and enthalpy changes obtained from PAC measurements exhibit smaller errors due to the better signal-to-noise ratio of the PAC signal as compared to the PBD signals. To

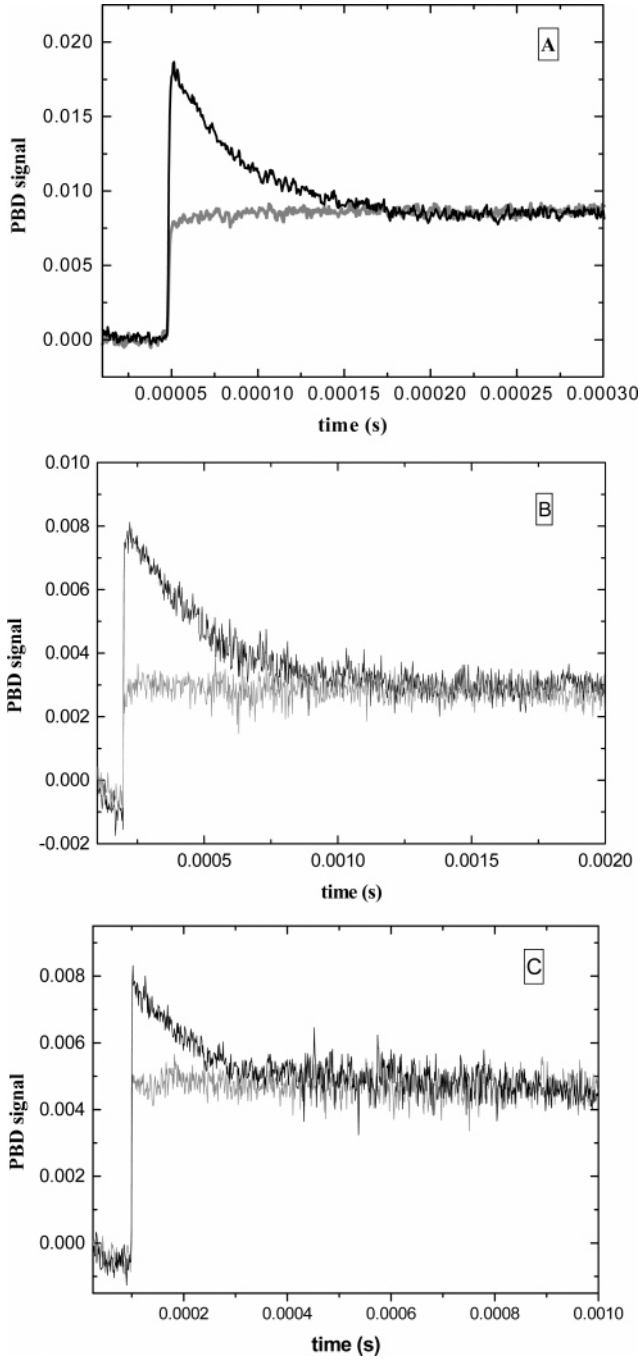

Figure 9. PBD traces obtained for CO photodissociation from and rebinding to (A) (CO)(H_2O)Fe^{II}4SP, (B) (CO)(2-MeIm)Fe^{II}4SP, and (C) (CO)Fe^{II}MP11 complexes at 16 °C. The black line represents a sample trace, and the gray line represents a reference trace. Each trace is an accumulation of 20−30 laser shots. The absorbance of the sample and the reference at the excitation wavelength (532 nm) was 0.4.

calculate the entropy changes reported in Table 1, we use the average values of the enthalpy changes obtained from PAC and PBD measurements along with the values of $\Delta G°$ obtained from steady-state absorption titrations.

From fits of the PBD sample traces to eq 8 the rate constants for ligand rebinding were obtained and used to determine activation enthalpies and activation entropies according to eq 9. The corresponding Eyring plots are shown in Figure 5, and extrapolated values are listed in Table 2. Activation enthalpy and entropy values determined from

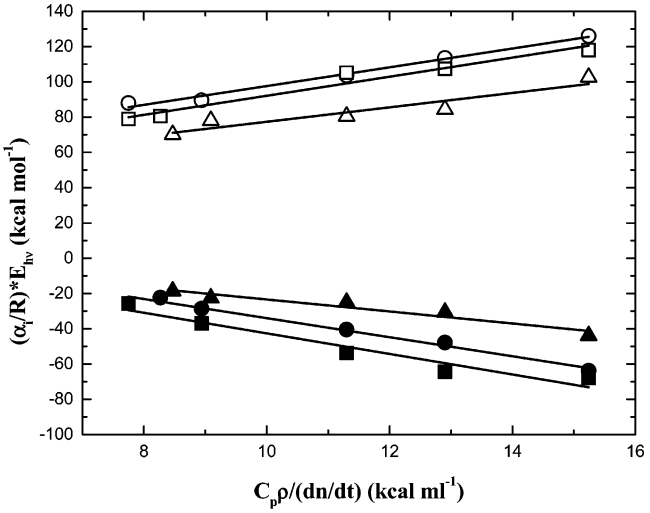

Figure 10. Plot of $\alpha_i/R^*E_{h\nu}$ versus $C_p\rho/(dn/dt)$ for CO photodissociation from and rebinding to $(H_2O)Fe^{II}4SP$ (circles), (2-MeIm)$Fe^{II}4SP$ (squares), and $Fe^{II}MP$-11 (triangles). α_i for the fast phase is shown as open symbols, and α_i for the slow phase is shown as solid symbols. The linear fits according to eq 7 are shown as a solid line.

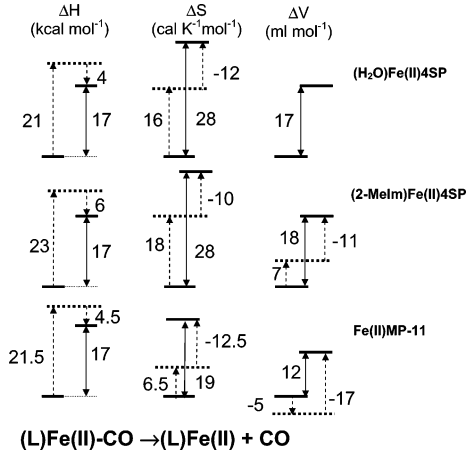

Figure 11. Enthalpy and volume profiles for CO dissociation from and rebinding to $(H_2O)Fe^{II}4SP$, (MeIM)$Fe^{II}4SP$, and $Fe^{II}MP$-11 complexes. Enthalpies of activation for ligand dissociation were determined from reaction enthalpies and activation enthalpy changes for CO rebinding using $\Delta H = \Delta H^{\ddagger}_f - \Delta H^{\ddagger}_r$. Activation volumes and entropies for ligand dissociation were determined by a similar way.

PBD measurements match those obtained from TA measurements within experimental error.

Discussion

The dynamics of CO dissociation and binding to various heme complexes have been extensively studied, and the "base elimination" mechanism for CO rebinding has been proposed.[6,9] According to this mechanism, CO photodissociation is followed by release of a proximal base leading to the formation of a four-coordinate heme. The four-coordinate intermediate recombines first with CO, and subsequent rebinding of the base represents the last step of the reaction. It has been observed that the rate constants of the individual steps depend on the type and concentration of the base and on the solvent.[6] For example, imidazole−Fe(II) deuteroporphyrin dimethylester in benzene exhibits a rate of base elimination of $\sim 2 \times 10^5$ s^{-1}. In CTAB solutions containing 1-methylimidazole the rate constant for base elimination was reported to be higher than 5×10^5 s^{-1}.[6] Huang et al. have studied the photolysis of a His−heme−CO complex in 80% glycerol.[9] In this system, the histidine base dissociates within 10 ps and its rebinding is the rate-limiting step. Alternately, increasing the local concentration of base and reducing the corresponding off-rate (through synthesis of chelated heme model compounds) results in direct association of CO to the five-coordinate heme.[7]

Using transient absorption spectroscopy, we have shown previously that CO photodisociation from $(CO)(H_2O)$-$Fe^{II}4SP$ leads to the formation of a five-coordinate complex $(H_2O)Fe^{II}4SP$ within 100 ns, and subsequent ligand rebinding occurs as a single-exponential step with a pseudo-first-order rate constant of 2.5×10^4 s^{-1} (1 mM CO).[11] The PAC and PBD results for the same complex presented here confirm our previous observation. In the PAC measurements only volume and enthalpy changes taking place within 50 ns after ligand photodissociation were detected and no additional kinetics between 50 ns and $\sim 5\ \mu$s were observed. On longer time scales, single exponential decay kinetics are observed in both TA and PBD measurements with nearly identical rate constants. Similarly, for (CO)(2-MeIm)$Fe^{II}4SP$ and $(CO)Fe^{II}MP11$ complexes only one phase on a time scale longer than 50 ns corresponding to CO rebinding was observed in both PBD and TA measurements. We propose that the mechanism for CO photodissociation and subsequent rebinding to (2-MeIm)$Fe^{II}4SP$ and $Fe^{II}MP11$ in water is the same as we have identified previously for $(H_2O)Fe^{II}4SP$[11] and can be described as

$$(CO)(L)Fe^{II}\text{heme} \xrightarrow{h\nu} CO + (L)Fe^{II}\text{heme} \rightarrow (CO)(L)Fe^{II}\text{heme}$$

Enthalpy, entropy, and volume profiles for CO rebinding to the three heme complexes are shown in Figure 11 and provide detailed insight into the ligand-rebinding mechanism. The reaction enthalpy and volume changes represent the average values of data obtained by PAC and PBD measurements, and the activation enthalpy and activation entropy values for ligand rebinding are the average values determined from PBD and TA measurements. Using reaction enthalpies for CO photodissociation (ΔH) and activation enthalpies for CO rebinding ($\Delta H^{\ddagger}_r$), the enthalpies of activation for CO photodissociation ($\Delta H^{\ddagger}_f$) were calculated according to

$$\Delta H = \Delta H^{\ddagger}_f - \Delta H^{\ddagger}_r \qquad (13)$$

In a similar fashion, the entropies of activation and activation volumes for the forward reaction were determined.

Observed reaction enthalpy changes are similar for all complexes and correspond well to enthalpy changes previously obtained for CO binding to chelated hemes ($\Delta H = -17$ kcal mol^{-1})[7] and to ferrous monohistidine-coordinated hemoprotein models ($\Delta H = -19$ kcal mol^{-1}),[22] consistent with a model in which only CO dissociates and rebinds to

(22) Lee, K.-H.; Kennedy, M. L.; Buchalova, M.; Benson, D. R. *Tetrahedron Lett.* **2000**, *56*, 9725−9731.

the heme on time scales longer than ~50 ns. Interestingly, the enthalpy of the CO−Fe bond is very similar for both the strong-field (2-MeIm) and weak-field (H_2O) proximal ligands. The enthalpy values parallel the CO binding constants which are nearly identical for (H_2O)Fe^{II}4SP and (2-MeIm)Fe^{II}4SP complexes (5.1×10^5 and 5.3×10^5 M^{-1}) indicating that the $\Delta G°$ values are also similar. These results are consistent with previous studies which report association constants for CO binding to deuterioheme in benzene in the presence of water or 2-methylimidazole as the proximal ligand to be roughly $K_a \sim 10^6$ M^{-1}.[23]

The activation enthalpy for CO rebinding to (H_2O)Fe^{II}4SP and to Fe^{II}MP-11 were observed to be 3.8 ± 0.5 and 4.5 ± 0.7 kcal mol^{-1}, respectively. Ligand recombination to the (2-MeIm)Fe^{II}4SP complex shows a higher activation barrier of roughly 2 kcal mol^{-1}, and the observed value ($\Delta H^{\ddagger}_r$ = 6.7 ± 0.6 kcal mol^{-1}) is similar to that obtained for reactions of CO with chelated protohemes ($\Delta H^{\ddagger}_r$ = 7.2 kcal mol^{-1}).[7] The larger activation enthalpy for the complex with 2-methylimidazole relative to the complex with water may originate from a larger displacement of the iron atom out of the heme plane and expansion of the porphyrin ring in the five-coordinate (2-MeIm)Fe^{II}4SP complex relative to the five-coordinate (H_2O)Fe^{II}4SP complex.[26] Interestingly, CO rebinding to the Fe^{II}MP11 complex with His in the proximal position is characterized by an enthalpy of activation smaller than that observed for the (2-MeIm)Fe^{II}4SP complex. In microperoxidase, the proximal ligand His18 is a part of a conformationally rigid pentapeptide segment Cys14−His18. The rigid position of His18 minimizes displacement of the iron atom out of the porphyrin plane during the high-spin to low-spin transition which contributes to the relatively low value of the activation enthalpy.

From the observed reaction enthalpies and calculated free energy changes the reaction entropy values for CO rebinding to all complexes were determined. They were found to be all negative: −28 cal K^{-1} mol^{-1} for (L)Fe^{II}4SP complexes and larger for Fe^{II}MP11 (−19 cal K^{-1} mol^{-1}). These values are roughly on the order of reaction entropy changes of −45 cal K^{-1} mol^{-1} previously proposed by Page and Jencks for bimolecular reactions due to the loss of translational and rotational degrees of freedom in solutions.[29] Entropies of activation are negative for all complexes and range between −10 and −14 cal K^{-1} mol^{-1}. The observed negative values of $\Delta S^{\ddagger}_r$ reflect a decrease in translational and rotational degrees of freedom associated with the transition state during CO rebinding.

In general, the reaction volume change can be described in terms of three contributions: van der Waals volume changes (ΔV_{vdW}); volume changes due to electrostriction (ΔV_{el}); volume changes due to solvation (ΔV_{sol}).[30,31] van der Waals volume changes include changes in bond lengths and angles during the reaction. Volume changes arising from solvent perturbation due to charge creation/destruction are described by the second term. The last term results from differences in solvent packing around the reactants and products. For example, fragmentation reactions are expected to have a positive contribution to ΔV_{sol} resulting from the increased molecular surface of the solutes exposed to the solvent.[32] We have determined that CO photodissociation is coupled to volume expansions of ~17 and ~12 mL mol^{-1} for the (L)Fe^{II}4SP and Fe^{II}MP-11 complexes, respectively. Upon CO photolysis $\Delta V_{el} = 0$, and thus, the observed $\Delta V = \Delta V_{vdW} + \Delta V_{sol}$. The origin of the expansion is attributed to Fe−CO bond cleavage and the low-spin to high-spin heme transition. It has been shown previously that the covalent bond breaking contributes a volume change of roughly 5−10 mL mol^{-1} [18,24] indicating that the spin interconversion contributes to the observed volume expansion by roughly 8 mL mol^{-1}. This value corresponds to reaction volumes measured for the low-spin to high-spin conversion in inorganic model systems. From equilibrium measurements, the reaction volume changes for spin transitions in Fe(II) tris(2-(2-pyridyl)imidazole) and Fe(II) tris(2-(2-pyridyl)-benzimidazole) in various solvents have been reported to range between 5 and 15 mL mol^{-1}.[25]

Structural changes associated with the heme which result from the low-spin to high-spin transition include an iron displacement out of the porphyrin plane of 0.3 Å and a contraction of the porphyrin core by 0.12 Å.[26] Such changes account for volume changes of −0.2 to −0.3 mL mol^{-1}.[27] Thus, the observed volume change of ~8 mL mol^{-1} appears to be much larger than that associated with the simple movement of iron out of the plane indicating that the observed volume changes originate primarily in the solvent perturbation due to the six-coordinate low-spin to five-coordinate high-spin transition. In the MP-11 complex, the presence of a pentapeptide fragment may partially reduce the solvent perturbation as evident from the smaller reaction volume change observed for this complex. The contribution from the solvation of the CO molecule upon photodissociation is expected to be small since CO is already partially solvated in the heme complexes.

Pressure dependence studies reveal that CO rebinding to (2-MeIm)Fe^{II}4SP and Fe^{II}MP-11 complexes is characterized by a negative volume of activation ~−11.4 ± 1.5 and −17.3 ± 2.5 mL mol^{-1}, respectively. Similar values were observed for all three complexes examined, and these values are close to those reported in early studies for CO rebinding to chelated protoheme ($\Delta V^{\ddagger}$ = −13.7 mL mol^{-1})[8,28] and CO rebinding to myoglobin ($\Delta V^{\ddagger}$ = −10 mL mol^{-1}).[35] Despite the fact that no direct thermodynamic equation links reaction/

(23) Rougee, M.; Braults, D. *Biochemistry* **1975**, *14*, 4100−4106.
(24) Hung, R. R.; Grabowski, J. J. *J. Am. Chem. Soc.* **1992**, *114*, 351−353.
(25) Hereman, K. In *High-Pressure Chemistry and Biochemistry*; van Eldik, R., Jonas, J., Eds.; D. Reidel Publishing Co.: Dordrecht, Holland, 1987.
(26) Collman, J. P. *Acc. Chem. Res.* **1997**, *10*, 2265−2272.
(27) Alden, G. A.; Satterlee, J. D.; Mintorovitch, J.; Constantinidis, I.; Ondrias, M. R.; Swanson, B. I. *J. Biol. Chem.* **1988**, *264*, 1933−1940.
(28) Taube, D. J.; Projahn, H. D.; van Eldik, R.; Magde, D.; Traylor, T. G. *J. Am. Chem. Soc.* **1990**, *112*, 6880−6886.
(29) Page, M. I.; Jencks, W. P. *Proc. Natl. Acad. Sci. U.S.A.* **1971**, *68*, 1678−1683.
(30) Schmidt, R.; Schutz, M. *Chem. Phys. Lett.* **1996**, *263*, 795−802.
(31) Yoshimura, Y.; Nakahara, J. *J. Chem. Phys.* **1984**, *81*, 4080−4086.
(32) Schmidt, R. *J. Phys. Chem.* **1998**, *102*, 9082−9086.

activation volume changes to reaction/activation entropy changes and vice versa, both quantities stem from the same source and thus some correlation between them is expected.[19] This is clearly evident here since the large negative $\Delta V/\Delta V^{\ddagger}$ values for the ligand rebinding correlates well with the determined negative $\Delta S/\Delta S^{\ddagger}$ values. The formation of the covalent bond is expected to contribute to the negative volume of activation by ~ -10 mL mol^{-1},[18,28,36] and the high-spin to low-spin transition in Fe(III) myoglobin was reported to be accompanied by a decrease in the volume of activation on the order of -10 to -15 mL mol^{-1}.[37] On the basis of the negative activation volume, CO rebinding can be best described by an associative mechanism with bond formation being the rate-limiting step. Thus, CO rebinding occurs via a direct mechanism previously suggested for CO rebinding to chelated hemes and to heme proteins. This conclusion is also supported by comparing the observed reaction volumes and enthalpies and the thermodynamic parameters determined for the CO photodissociation reaction from protoporphyrin IX encapsulated in CTAB micelles.[10] In that system, CO dissociation occurs via a base elimination mechanism resulting in the formation of a four-coordinate heme within 100 ns. Distinct from the results presented here, in the CTAB/protoheme IX system, the reaction is exothermic ($\Delta H = -10$ kcal mol^{-1}) and exhibits a small reaction volume change of $\sim$3 mL mol^{-1} and a positive volume of activation for CO rebinding of 3.7 mL mol^{-1}.

Acknowledgment. The authors acknowledge the National Science Foundation (R.W.L., Grant MCB0317334) and the American Heart Association (R.W.L., Grant AHA0255037B).

IC048963C

(33) Scheidt, W. R.; Ellison, M. K. *Iron Porphyrins*; Addison-Wesley: Reading, MA, 1983; Part 1.
(34) Wegewijs, B.; Paddon-Row, M. N.; Braslavsky, S. E. *J. Phys. Chem.* **1998**, *102*, 8812−8818.
(35) Projahn, H. D.; van Eldik, R. *Inorg. Chem.* **1991**, *30*, 3288−3293.
(36) Le Noble, W. R. *Prog. Phys. Org. Chem.* **1965**, *5*, 207.
(37) Morishima, I.; Ogawa, S.; Yamada, H. *Biochemistry* **1980**, *19*, 1569.